

# Atom Interferometer Phase Shear and Spacetime Sectional Curvature

Hunter Swan<sup>\*</sup> and Jason M. Hogan<sup>†</sup>

*Department of Physics, Stanford University, Stanford, California 94305, USA*

(Dated: September 1, 2025)

Atom interferometry is a natural laboratory for precision tests of general relativity, but there is no simple relationship between atom interferometer phase and geometric properties of spacetime. Here we show that a different atom interferometer observable, the phase shear, can be expressed directly as the integrated sectional curvature over a spacetime surface enclosed by the interferometer arms and final beamsplitter. This is a consequence of a generalized Gauss-Bonnet theorem, which also explicitly computes small correction terms arising from gravitational redshift of atom optics pulses. This synthesis of quantum mechanics, relativity, and differential geometry affords a manifestly coordinate-free and representation-free means of measuring spacetime properties. Additionally, it provides a convenient computational tool for predicting atom interferometer properties in arbitrary background spacetimes.

From its earliest days, atom interferometry has been understood to be an excellent technique for precision measurement of gravity [1]. Recent years have seen a rapid development of atom interferometer (AI) technology for such applications as geodesy [2, 3], gravitational wave detection [4–7], and weak equivalence principle tests [8–12]. Various formalisms exist for describing observable AI features [13–17], but the relationship between these features and intrinsic geometric properties of spacetime is often opaque. This is due partly to the confounding influence of non-gravitational effects and partly to the algebraic difficulty of modeling typical AI geometries.

The main observable in an AI is the phase  $\Delta\phi$ , which decomposes in a relativistically covariant way as [13]

$$\Delta\phi = \Delta\phi_{\text{prop}} + \Delta\phi_{\text{laser}} + \Delta\phi_{\text{sep}}. \quad (1)$$

The propagation phase  $\Delta\phi_{\text{prop}}$  and separation phase  $\Delta\phi_{\text{sep}}$  depend on the geodesic trajectories of the interferometer arms and atom optic light pulses, and thus depend indirectly on spacetime geometry, whereas the laser phase  $\Delta\phi_{\text{laser}}$  depends also on the evolution of the laser generating the pulses. Laser phase may be considered a parasitic effect to measurement of spacetime curvature, and the gradiometric configuration of [5] was designed to remove this effect via a differential measurement between two AIs. Even in such a gradiometer, it remains a significant challenge to compute differential phase in a known spacetime geometry, or conversely to infer spacetime geometry from measured differential phases. In addition to these difficulties, the terms  $\Delta\phi_{\text{prop}}$ ,  $\Delta\phi_{\text{laser}}$ , and  $\Delta\phi_{\text{sep}}$  are not separately observable, with other representations decomposing the observable  $\Delta\phi$  in different ways [14, 18–22], leading to interest in which elements of an AI phase calculation are in fact physically meaningful [23].

In this work, we show that in contrast to  $\Delta\phi$ , the *phase shear* of an AI has a direct geometric meaning related to integrated sectional curvature over a spacetime surface bounded by the interferometer arms and final beamsplitter (FBS). Phase shear arises due to a momentum difference between the interferometer arms after the FBS, i.e.

a failure to close in momentum space, and manifests as a periodic modulation of the interferometer output ports. Phase shear due to a gravity gradient has been measured experimentally [24] and is an important effect for AI weak equivalence principle tests [25].

Our basic result states that if an AI is designed such that in flat space the momentum difference  $\Delta p$  between the two wavepackets in a given output port would vanish, then applying the same laser pulse sequence to an AI in curved space will lead to a momentum difference

$$\Delta p = -mc \int_M K \, dA + \mathcal{O}(m\bar{v}\bar{K}\bar{A}), \quad (2)$$

where  $m$  is the atom mass,  $c$  the speed of light,  $M$  a spacetime surface bounded by the AI arms and FBS,  $K$  the sectional curvature on  $M$ , and  $dA$  the area element on  $M$ . The notation  $\mathcal{O}(x)$  indicates additional terms of typical magnitude  $x$  or smaller, and  $\bar{v}$ ,  $\bar{K}$ ,  $\bar{A}$  are characteristic scales for the atomic recoil velocity, spacetime sectional curvature, and spacetime area, respectively. The magnitude of  $m\bar{v}\bar{K}\bar{A}$  is smaller than the first term in Eq. (2) by  $\bar{v}/c$ , which is typically  $\sim 10^{-11}$ . We will show how to compute the error explicitly and see that it arises primarily from gravitational redshift of atom optics photons. We emphasize Eq. (2) applies equally to multi-photon atom optics (such as Bragg or Raman transitions) or single-photon atom optics [5]. The momentum difference  $\Delta p$  induces a modulation on the AI output port with wavelength  $\lambda = \frac{h}{\Delta p}$ , where  $h$  is Planck’s constant. The observability of this effect depends roughly on whether this modulation wavelength is smaller than the AI atom cloud size, which is typically a few millimeters. We note that phase shear can also arise in a qualitatively different way when the AI wavepackets have significant phase curvature, as in [26]. We do not consider this effect here, assuming all wavepackets are collimated so as to have negligible phase curvature and focusing solely on phase shear arising from wavepacket momentum differences.

We later will discuss variants of this basic setup requiring only simple modifications of the above result. For in-

stance, in [24, 25] phase shear is eliminated by a judicious frequency offset of the central mirror pulse, and space-time curvature is then measured by this frequency offset rather than phase shear. In derivations below we adopt natural units  $c = \hbar = 1$ . We will reinsert dimensional constants when we consider specific examples.

Our main technical tool is a generalized version of the Gauss-Bonnet (GB) theorem. Many authors [27–30] have introduced Lorentzian versions of GB, though most exclude null boundary segments. We use a formalism similar to [28, 30], but modified to allow null geodesics, as described in Appendix A. This relativistic GB formula states that, given a piecewise smooth curve  $\gamma$  bounding a 1+1 dimensional Lorentzian surface  $M$ , under appropriate technical hypotheses we have

$$\int_M K dA + \oint_\gamma k_g ds + \sum_j \alpha_j = 0, \quad (3)$$

where  $K$  is sectional curvature,  $k_g$  is geodesic curvature along  $\gamma$ ,  $dA$  is the area element on  $M$ ,  $ds$  is differential proper time along  $\gamma$ , and  $\alpha_j$  is an “angle” (to be defined below) associated to each non-smooth point  $P_j$  on  $\gamma$ .

The sectional curvature and geodesic curvature terms of Eq. (3) are identical to the usual (Riemannian) GB formula [31], but care is needed to define a notion of angle on a Lorentzian manifold. Given two time-like future directed unit vectors  $S, T$  at a point  $P \in M$ , we define the angle  $\alpha$  from  $S$  to  $T$  to be the boost angle (i.e. rapidity) of a Lorentz transformation  $L(\alpha)$  acting on the tangent space  $\mathbf{T}_P M$  which maps  $S$  to  $T$ . Recall that with respect to an orthonormal basis for  $\mathbf{T}_P M$ ,  $L(\alpha)$  takes the form

$$L(\alpha) = \begin{pmatrix} \cosh(\alpha) & \sinh(\alpha) \\ \sinh(\alpha) & \cosh(\alpha) \end{pmatrix}. \quad (4)$$

For an arbitrary non-null vector  $S \in \mathbf{T}_P M$ , let  $\hat{S}$  denote the unique time-like future directed unit vector in  $\mathbf{T}_P M$  which is either parallel to  $S$  (if  $S$  is time-like) or orthogonal to  $S$  (if  $S$  is space-like). Then given any two such non-null vectors  $S, T \in \mathbf{T}_P M$ , the angle from  $S$  to  $T$  is defined to be the angle from  $\hat{S}$  to  $\hat{T}$ . Angles so defined have an additivity property: The angle from  $S$  to  $T$  plus the angle from  $T$  to  $U$  equals the angle from  $S$  to  $U$ .

Given two time-like vectors  $S$  and  $T$ , the angle from  $S$  to  $T$  can be conveniently evaluated in the rest frame of  $S$ , i.e. the local Lorentz frame such that  $\hat{S}$  has components  $(1, 0)^\top$ . Let  $T$  have components  $(T_t, T_x)^\top$  in this frame. Then the angle from  $S$  to  $T$  is given by  $\tanh^{-1}(T_x/T_t)$ .

Finally, we consider angles associated to null geodesics (see Fig. 1). Suppose that null geodesic segment  $\gamma_1$  intersects two non-null curves  $\gamma_0$  and  $\gamma_2$  at points  $P_1, P_2$  respectively, and define a single angle  $\alpha$  for these two points as follows. Take the tangent vector  $S$  to  $\gamma_0$  at  $P_1$  and the tangent vector  $T$  to  $\gamma_2$  at  $P_2$  and parallel transport both along the null geodesic  $\gamma_1$  to any common point. Write the parallel transported vectors  $\tilde{S}, \tilde{T}$

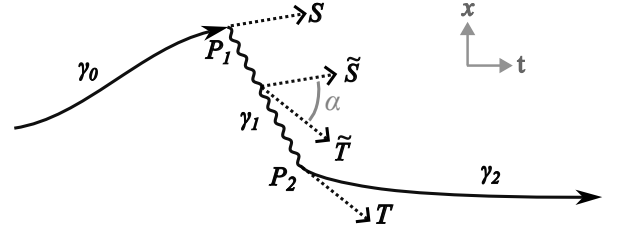


FIG. 1. Defining angle  $\alpha$  at a null geodesic  $\gamma_1$  by parallel transport of tangent vectors. The wavy line is a null geodesic, solid lines are time-like curves, and dotted lines are tangent vectors.  $\alpha$  is defined to be the angle from  $\tilde{S}$  to  $\tilde{T}$ .

and define  $\alpha$  to be the angle from  $\tilde{S}$  to  $\tilde{T}$ . This definition is independent of the specific point along  $\gamma_1$  chosen. For convenience, in the context of Eq. (3) we define the angle of the initial endpoint of a null geodesic to be this  $\alpha$  and the angle of the final endpoint to be zero.

More general notions of Lorentzian angle are possible [27], but that above is convenient and sufficient for our purpose. With these definitions, Eq. (3) holds provided all null segments of  $\gamma$  are geodesic and no two null segments are adjacent. See Appendix A for more details.

Before applying Eq. (3) to an AI, we recall some standard relationships between boost angle and momentum. Consider a particle  $\Pi$  with mass  $m$  and unit tangent vector  $T$ , and let  $S$  be any other time-like future directed vector at the same point. Let  $\alpha$  be the angle from  $S$  to  $T$ . In the rest frame of  $S$ , the velocity of  $\Pi$  is  $\tanh(\alpha)$  and the momentum of  $\Pi$  has components  $m(\cosh(\alpha), \sinh(\alpha))^\top$ , so that the spatial component is

$$p = m \sinh(\alpha) = m\alpha + \mathcal{O}(m\alpha^3). \quad (5)$$

If  $\Pi$  absorbs a photon with momentum  $(\nu, \nu)^\top$  in the rest frame of  $T$ , its final momentum is  $(m + \nu, \nu)^\top$ , and its recoil velocity  $v$  is  $\nu/(m + \nu)$ , which has typical magnitude  $\sim 2 \times 10^{-11}$  for e.g. the 698 nm clock transition in  $^{87}\text{Sr}$ . The angle from initial to final momentum of  $\Pi$  is

$$\beta = \tanh^{-1}\left(\frac{\nu}{m + \nu}\right) = \frac{\nu}{m + \nu} + \mathcal{O}(\bar{v}^3). \quad (6)$$

Similarly, if  $\Pi$  then emits an identical photon, it experiences a boost  $-\beta$ . For a multi-photon transition, one has a similar relation to Eq. (6) with  $(\nu, \nu)^\top$  replaced by the effective momentum of the transition. If the photon momentum is given by  $(\nu, \nu)^\top$  in the rest frame of  $S$  rather than  $T$ , we compute the resulting boost to  $\Pi$  by first expressing the momentum in the rest frame of  $T$  as

$$L(-\alpha) \begin{pmatrix} \nu \\ \nu \end{pmatrix} = \begin{pmatrix} e^{-\alpha} \nu \\ e^{-\alpha} \nu \end{pmatrix} \quad (7)$$

and then applying Eq. (6).

We now apply Eq. (3) to an AI, as shown schematically in Fig. 2. We follow the covariant semiclassical formalism

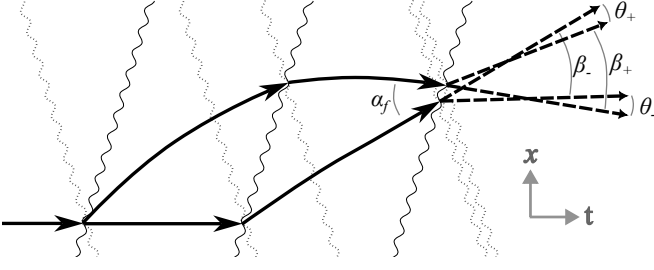


FIG. 2. Typical Mach-Zehnder atom interferometer. Dashed lines are output port atom wavepackets. Solid wavy lines are null geodesics for a single-photon AI, and hatched wavy lines indicate additional null geodesics in a two-photon AI.

of [13] in describing the AI. The upper and lower output ports of the AI both consist of two wavepackets arising from the two AI arms, and the phase shear of the upper (lower) output port can be characterized by a boost angle  $\theta_+$  ( $\theta_-$ ) between these two wavepackets along the final beamsplitter null geodesic. We refer to  $\theta_{\pm}$  as a *shear angle*, and it determines the momentum difference  $\Delta p$  between the output port wavepackets via Eq. (5). Note that generically  $\theta_+ \neq \theta_-$ , leading to (slightly) different phase shear between the two output ports.

We set  $\gamma$  in Eq. (3) to consist of the lower AI arm, followed by the FBS null geodesic segment connecting the two arms, followed by the upper arm traversed backwards. Since all boundary segments are geodesic, geodesic curvature is uniformly zero on  $\gamma$ , and Eq. (3) relates angles on  $\gamma$  (a type of holonomy of  $\gamma$ ) to the enclosed sectional curvature. Let  $\alpha_f$  denote the angle across the FBS, and let  $-\beta_-$  ( $\beta_+$ ) be the boost imparted to the lower (upper) arm by the FBS. Note that  $\beta_{\pm}$  is not an angle of  $\gamma$ , but is needed to compute the shear angle  $\theta_{\pm}$ , which is given by

$$\theta_{\pm} = \alpha_f - \beta_{\pm}. \quad (8)$$

We consider the typical case where the atom optics pulses are designed such that the shear angle would vanish for an AI in flat space, and examine what the shear angle must be for an AI in curved space with atom optics pulses of the same order, direction, and frequency at point of emission. Since we need to refer to analogous quantities in both flat space and curved space AIs, we adopt the convention that unprimed symbols such as  $\alpha_f, \theta_+$  refer to a curved space AI, while primed quantities  $\alpha'_f, \theta'_+$  refer to analogous quantities in a flat space AI, and a differential quantity like  $\Delta\alpha_f$  will denote  $\alpha_f - \alpha'_f$ .

In the flat space AI, Eq. (3) becomes

$$\sum_j \alpha'_j = 0 \quad (9)$$

since  $K' = 0$ . In curved space, Eqs. (3) and (9) give

$$0 = \int_M K dA + \sum_j \alpha_j = \int_M K dA + \sum_j \Delta\alpha_j. \quad (10)$$

Solving for  $\Delta\alpha_f$ ,

$$\Delta\alpha_f = - \int_M K dA - \sum_{j \neq f} \Delta\alpha_j, \quad (11)$$

which together with  $\theta'_{\pm} = 0$  gives the shear angle

$$\begin{aligned} \theta_{\pm} &= \alpha_f - \beta_{\pm} = \Delta\alpha_f - \Delta\beta_{\pm} \\ &= - \int_M K dA - \sum_{j \neq f} \Delta\alpha_j - \Delta\beta_{\pm}. \end{aligned} \quad (12)$$

It remains to compute  $\Delta\alpha_j$  for  $j \neq f$  and  $\Delta\beta_{\pm}$ . Note that  $\alpha_j$  ( $j \neq f$ ) and  $\beta_{\pm}$  depend only on the frequency of the atom optic photon at the point of interaction, as in Eq. (6), unlike  $\alpha_f$ , which depends on the relative motion of the two AI arms at the FBS. Thus  $\Delta\beta_{\pm}$ ,  $\Delta\alpha_j$  depend only on the change in photon frequency due to spacetime curvature, i.e. gravitational redshift.

We will sketch how to compute  $\Delta\alpha_j$  via Eq. (3) applied to a loop bounded by the trajectories of the atom, the laser emitting the light pulses, and certain atom optics, and show that  $\Delta\alpha_j$  is much smaller than  $\int_M K dA$ . For clarity, we work only to leading order in all small parameters, but this is not an essential limitation. We allow the laser to follow a non-geodesic trajectory (e.g. fixed to Earth's surface), but suppose that its geodesic curvature is identical in the curved and flat space AIs, i.e.  $k_g = k'_g$ . We further suppose for simplicity that the AI initial conditions are such that the angle  $\phi_0$  across the initial beamsplitter (IBS) from the laser to lower AI arm is identical between curved and flat space, i.e.  $\phi_0 = \phi'_0$ .

Let  $\alpha_1$  denote the boost imparted to the lower AI arm by the first atom optic after the IBS, and let  $\phi_1$  denote the angle from laser to incoming atom across this atom optic null geodesic, as in Fig. 3. Letting  $N_1$  denote the surface bounded by this atom optic along with the laser, atom, and IBS, Eq. (3) gives

$$\phi'_1 = \phi_0 - \int_{\text{laser}} k_g ds, \quad (13)$$

$$\phi_1 = \phi_0 - \int_{\text{laser}} k_g ds - \int_{N_1} K dA. \quad (14)$$

Let  $(\nu, \nu)^{\top}$  be the momentum of the photon inducing  $\alpha_1$  in the rest frame of the laser. From Eq. (7), the photon momentum in the atom's rest frame is  $(e^{-\phi_1}\nu, e^{-\phi_1}\nu)^{\top}$ . From Eq. (6), the atom's boost is

$$\alpha'_1 = \tanh^{-1} \left( \frac{e^{-\phi'_1}\nu}{m + e^{-\phi'_1}\nu} \right) \quad (15)$$

$$\alpha_1 = \tanh^{-1} \left( \frac{e^{-\int_{N_1} K dA} e^{-\phi'_1}\nu}{m + e^{-\int_{N_1} K dA} e^{-\phi'_1}\nu} \right) \quad (16)$$

Finally, expanding to leading order in  $\int_{N_1} K dA$  we find

$$\Delta\alpha_1 = -\alpha'_1 \int_{N_1} K dA + \mathcal{O}(\bar{v}^2 \bar{K} \bar{A} + \bar{v} \bar{K}^2 \bar{A}^2). \quad (17)$$

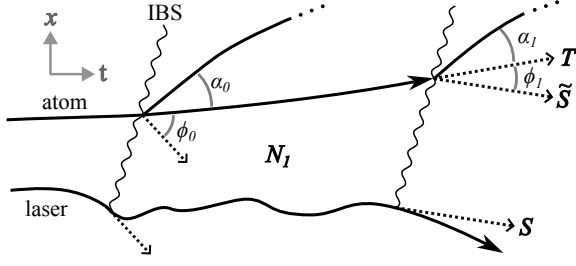


FIG. 3. Spacetime loop for computing the redshift of an atom optic light pulse. The laser trajectory is shown with wiggles to emphasize that it may follow a non-geodesic trajectory.

In all examples below it will be true that  $\left| \int_{N_1} K dA \right| \ll 1$ , justifying the expansion. We see that  $\Delta\alpha_1$  has the same form as the leading term  $\int_M K dA$  of Eq. (12), integrated over a possibly larger surface  $N_1$  but suppressed by  $\alpha'_1$ , which is  $\mathcal{O}(\bar{v})$ . Subsequent terms  $\Delta\alpha_j$  and  $\Delta\beta_{\pm}$  may be computed similarly, inductively taking into account the previous angles, with the same leading order result

$$\Delta\alpha_j = -\alpha'_j \int_{N_j} K dA + \mathcal{O}(\bar{v}^2 \bar{K} \bar{A} + \bar{v} \bar{K}^2 \bar{A}^2), \quad (18)$$

$N_j$  now being a surface bounded by the relevant atom optic, IBS, atom and laser. Together with Eqs. (5) and (12), this yields a refined version of our main result Eq. (2),

$$\begin{aligned} \Delta p_{\pm} = & -m \int_M K dA - m \sum_{j \neq f} \alpha'_j \int_{N_j} K dA \\ & + m \beta'_{\pm} \int_{N_{\pm}} K dA + \mathcal{O}(\bar{K}^3 \bar{A}^3 + \bar{v}^2 \bar{K} \bar{A} + \bar{v} \bar{K}^2 \bar{A}^2), \end{aligned} \quad (19)$$

where the shear may now differ slightly between the two output ports. We will not analyze the new correction terms in detail, but note that the alternating sign of  $\alpha'_j$  for different  $j$  will lead to significant cancellation.

We highlight a few variations of this argument. Firstly, we have considered a comparison to an AI in flat space, but one could equally well compare to any reference background spacetime. If atom optics are designed to yield zero phase shear in such a reference spacetime, then observation of phase shear in an unknown spacetime reveals deviation of the real sectional curvature from that of the reference. Secondly, in the case of multi-loop or resonant AIs in which the arms cross [32], one must account for the orientation of spacetime area, which varies with the handedness of the boundary region, but the above argument is otherwise unchanged. Thirdly, in the configuration of [24, 25], the central mirror pulse is detuned so that phase shear vanishes. Here  $\theta_{\pm} = 0$  and instead

$$\Delta\alpha_{\pi\pm} = \pm \frac{1}{2} \int_{M'} K dA + \mathcal{O}(\bar{v} \bar{K} \bar{A}), \quad (20)$$

where  $\pi+$  ( $\pi-$ ) indexes the upper (lower) mirror pulse angle in Eq. (12). From Eqs. (6) and (7), the frequency

shift  $\Delta\nu$  which realizes this is  $m\Delta\alpha_{\pi-}$  to leading order. Thus  $\Delta\nu$  measures spacetime curvature in this case. Note that in a single photon AI, this configuration inevitably entails loss of contrast due to diminished mirror pulse efficiency. One mitigation strategy is to apply smaller detunings to a larger number of pulses: Since pulse efficiency varies as  $\Delta\nu^2$ , detuning  $N$  pulses by  $\Delta\nu/N$  results in a factor of  $N$  improvement in contrast. Lastly, if the phase shear modulation wavelength is comparable to the atom cloud size, measurement can be enhanced by introducing *artificial shear* (cf. [24, 26]), e.g. by frequency shifting the FBS, which simply adds a known offset to the shear induced by spacetime curvature.

As a first application, for weak gravity the sectional curvature integral of Eq. (2) may be evaluated to leading order by integrating over the region bounded by the unperturbed atom and photon trajectories. Moreover, in linearized gravity, a static Newtonian metric

$$ds^2 = (1 + 2\Phi(x)) dt^2 - (1 - 2\Phi(x)) dx^2 \quad (21)$$

has sectional curvature  $\Phi''(x)$ , reproducing a known result that phase shear measures gravity gradients [24, 25].

Next we consider the Schwarzschild metric, with sectional curvature in the  $r$ - $t$  plane  $K = -r_s/r^3$ , for  $r$  the radial coordinate and  $r_s$  the Schwarzschild radius. At Earth's surface,  $r_s \approx 8.9$  mm and  $r \approx 6.4 \times 10^6$  m, so approximating  $c^2 K \approx 3100$  eotvos as constant over the AI, the resulting phase shear wavelength is

$$\lambda = \frac{h}{mcKA} \approx 1.5 \text{ mm} \left( \frac{1 \text{ m s}}{A/c} \right), \quad (22)$$

for  $m = 87$  amu. This is readily observable for a few mm atom cloud size and a spacetime area  $A/c \sim 1$  m s. Similarly, phase shear from test masses [33] can also be observable. The sectional curvature at the surface of a spherical test mass of density  $\rho$  is  $-2G_N\rho$  (where  $G_N$  is Newton's constant), or  $\sim 11000$  eotvos for Tungsten. This is measurable for an AI of spacetime area  $\sim 1$  m s near the test mass, which could be achieved via e.g. a levitation sequence or co-moving test mass.

For long baseline terrestrial gradiometers, the *differential* phase shear between the two AIs may be measurable. For a vertical gradiometer at Earth's surface with baseline 1 km and spacetime area of 1000 m s for each AI, such as proposed future versions of MAGIS [7], the difference in sectional curvature  $\Delta K$  between the two AIs is  $c^2 \Delta K \approx 1.4$  eotvos. Thus if the shear of one AI is made zero as in [25], the other will exhibit shear of wavelength  $\approx 3.2$  mm. This may be a significant effect in future long baseline detectors.

We note gravitational waves are not likely to produce measurable phase shear. The sectional curvature of a gravitational wave is of order  $c^2 \omega^2 h$ , with  $h$  the strain and  $\omega$  the angular frequency. For reasonable values  $h \sim 10^{-21}$  and  $\omega \sim 2\pi \times 1$  Hz,  $c^2 K \sim 3 \times 10^{-11}$  eotvos, 14 orders of magnitude smaller than that at Earth's surface.



Lastly, we consider the effect of laser frequency noise. An atom optic frequency offset  $\Delta\omega$  alters the AI boost angle by  $\Delta\omega/m$  (cf. Eq. (20)). Laser frequency noise  $\Delta\omega \sim 2\pi \times 10^3 \text{ s}^{-1}$  would induce spurious phase shear of wavelength  $2\pi c/\Delta\omega \sim 10^5 \text{ m}$ , which is safely unobservable. For an  $N$  pulse large momentum transfer sequence this wavelength may be reduced by a factor of  $\sim \sqrt{N}$ , but is likely still unobservable for all proposed AI experiments, for which  $N \sim 10^4$  is considered optimistic.

Summarily, we have shown that phase shear of a collimated atom interferometer has a direct geometric interpretation as the integrated sectional curvature over the spacetime surface bounded by the interferometer arms and final beamsplitter null geodesic. Phase shear thus provides a measurement of spacetime geometry which is independent of interferometer phase, is robust to noise, and applies equally to single-photon and multi-photon AIs. This interpretation facilitates calculation of phase shear in non-trivial metrics. We have provided several examples where this effect is likely to be observable or already observed. The geometric interpretation of atom interferometer phase shear thus provides an elegant and powerful theoretical tool for understanding the connection between gravitation and atom interferometry.

## ACKNOWLEDGEMENTS

This work was supported by the National Science Foundation QLCI Award No. OMA-2016244 and the Gordon and Betty Moore Foundation Grant GBMF7945.

---

\* orswan@stanford.edu

† hogan@stanford.edu

- [1] M. Kasevich and S. Chu, Measurement of the gravitational acceleration of an atom with a light-pulse atom interferometer, *Applied Physics B* **54**, 321 (1992).
- [2] A. Peters, K. Y. Chung, and S. Chu, High-precision gravity measurements using atom interferometry, *Metrologia* **38**, 25 (2001).
- [3] J. Stockton, K. Takase, and M. Kasevich, Absolute geodetic rotation measurement using atom interferometry, *Phys. Rev. Lett.* **107**, 133001 (2011).
- [4] S. Dimopoulos, P. W. Graham, J. M. Hogan, M. A. Kasevich, and S. Rajendran, Gravitational wave detection with atom interferometry, *Physics Letters B* **678**, 37 (2009).
- [5] P. W. Graham, J. M. Hogan, M. A. Kasevich, and S. Rajendran, New method for gravitational wave detection with atomic sensors, *Phys. Rev. Lett.* **110**, 171102 (2013).
- [6] S. Dimopoulos, P. W. Graham, J. M. Hogan, M. A. Kasevich, and S. Rajendran, Atomic gravitational wave interferometric sensor, *Phys. Rev. D* **78**, 122002 (2008).
- [7] M. Abe, P. Adamson, M. Borcean, D. Bortoletto, K. Bridges, S. P. Carman, S. Chattopadhyay, J. Coleman, N. M. Curfman, K. DeRose, *et al.*, Matter-wave atomic gradiometer interferometric sensor (MAGIS-100), *Quantum Science and Technology* **6**, 044003 (2021).
- [8] A. Bonnin, N. Zahzam, Y. Bidel, and A. Bresson, Simultaneous dual-species matter-wave accelerometer, *Phys. Rev. A* **88**, 043615 (2013).
- [9] D. Schlippert, J. Hartwig, H. Albers, L. L. Richardson, C. Schubert, A. Roura, W. P. Schleich, W. Ertmer, and E. M. Rasel, Quantum test of the universality of free fall, *Phys. Rev. Lett.* **112**, 203002 (2014).
- [10] M. G. Tarallo, T. Mazzoni, N. Poli, D. V. Sutyryn, X. Zhang, and G. M. Tino, Test of einstein equivalence principle for 0-spin and half-integer-spin atoms: Search for spin-gravity coupling effects, *Phys. Rev. Lett.* **113**, 023005 (2014).
- [11] L. Zhou, S. Long, B. Tang, X. Chen, F. Gao, W. Peng, W. Duan, J. Zhong, Z. Xiong, J. Wang, Y. Zhang, and M. Zhan, Test of equivalence principle at  $10^{-8}$  level by a dual-species double-diffraction raman atom interferometer, *Phys. Rev. Lett.* **115**, 013004 (2015).
- [12] P. Asenbaum, C. Overstreet, M. Kim, J. Curti, and M. A. Kasevich, Atom-interferometric test of the equivalence principle at the  $10^{-12}$  level, *Phys. Rev. Lett.* **125**, 191101 (2020).
- [13] S. Dimopoulos, P. W. Graham, J. M. Hogan, and M. A. Kasevich, General relativistic effects in atom interferometry, *Phys. Rev. D* **78**, 042003 (2008).
- [14] L. Badurina, Y. Du, V. S. Lee, Y. Wang, and K. M. Zurek, Signatures of linearized gravity in atom interferometers: A simplified computational framework, *Physical Review D* **111**, 042002 (2025).
- [15] M. Werner, P. K. Schwartz, J.-N. Kirsten-Siemß, N. Gaaloul, D. Giulini, and K. Hammerer, Atom interferometers in weakly curved spacetimes using Bragg diffraction and Bloch oscillations, *Phys. Rev. D* **109**, 022008 (2024).
- [16] A. Roura, Atom interferometer as a freely falling clock for time-dilation measurements, *Quantum Science and Technology* **10**, 025004 (2025).
- [17] A. Roura, Gravitational redshift in quantum-clock interferometry, *Phys. Rev. X* **10**, 021014 (2020).
- [18] A. Roura, W. Zeller, and W. P. Schleich, Overcoming loss of contrast in atom interferometry due to gravity gradients, *New Journal of Physics* **16**, 123012 (2014).
- [19] C. Ufrecht and E. Giese, Perturbative operator approach to high-precision light-pulse atom interferometry, *Physical Review A* **101**, 053615 (2020).
- [20] P. Storey and C. Cohen-Tannoudji, The Feynman path integral approach to atomic interferometry. a tutorial, *Journal de Physique II* **4**, 1999 (1994).
- [21] C. Antoine and C. J. Bordé, Exact phase shifts for atom interferometry, *Physics Letters A* **306**, 277 (2003).
- [22] B. Dubetsky, S. B. Libby, and P. Berman, Atom interferometry in the presence of an external test mass, *Atoms* **4**, 14 (2016).
- [23] C. Overstreet, P. Asenbaum, and M. A. Kasevich, Physically significant phase shifts in matter-wave interferometry, *American Journal of Physics* **89**, 324 (2021).
- [24] C. Overstreet, P. Asenbaum, T. Kovachy, R. Notermans, J. M. Hogan, and M. A. Kasevich, Effective inertial frame in an atom interferometric test of the equivalence principle, *Physical review letters* **120**, 183604 (2018).
- [25] A. Roura, Circumventing Heisenberg's uncertainty principle in atom interferometry tests of the equivalence principle, *Physical review letters* **118**, 160401 (2017).

- [26] A. Sugarbaker, S. M. Dickerson, J. M. Hogan, D. M. Johnson, and M. A. Kasevich, Enhanced atom interferometer readout through the application of phase shear, *Physical review letters* **111**, 113002 (2013).
- [27] G. Helzer, A relativistic version of the Gauss-Bonnet formula, *Journal of Differential Geometry* **9**, 507 (1974).
- [28] G. S. Birman and K. Nomizu, The Gauss-Bonnet theorem for 2-dimensional spacetimes, *The Michigan mathematical journal* **31**, 77 (1984).
- [29] Dzan Jin Jee, Gauss-Bonnet formula for general Lorentzian surfaces, *Geometriae Dedicata* **15**, 215 (1984).
- [30] P. R. Law, Neutral geometry and the Gauss-Bonnet theorem for two-dimensional pseudo-Riemannian manifolds, *The Rocky Mountain Journal of Mathematics* **22**, 1365 (1992).
- [31] N. J. Hicks, *Notes on differential geometry* (van Nostrand Princeton, 1965).
- [32] P. W. Graham, J. M. Hogan, M. A. Kasevich, and S. Rajendran, Resonant mode for gravitational wave detectors based on atom interferometry, *Physical Review D* **94**, 104022 (2016).
- [33] C. Overstreet, P. Asenbaum, J. Curti, M. Kim, and M. A. Kasevich, Observation of a gravitational Aharonov-Bohm effect, *Science* **375**, 226 (2022).

## APPENDIX A

Our definition of Lorentzian angles between non-null vectors is equivalent to that of Helzer [27] or the real part only of the definition of Law [30], and is equivalent to the definition of Birman and Nomizu [28] for time-like vectors. We will show that the Gauss-Bonnet formula as given by Law [30] can be extended to incorporate our definition of angles across null geodesics. Helzer's notion of angle is more general still, but we find the definition via parallel transport convenient for application to an AI final beamsplitter, where the ultimate goal is to compare two time-like momenta.

Taking the real part only of the Gauss-Bonnet formula of [30] yields precisely our Eq. (3). Suppose the boundary loop  $\gamma$  consists of smooth segments  $\gamma_j$ ,  $j = 0, \dots, n-1$ . Let  $P_j$  denote the common endpoint of  $\gamma_{j-1}$  and  $\gamma_j$  (with  $j-1$  taken mod  $n$ ) and let  $\tau_j$  denote the corresponding parameter time such that  $P_j = \gamma(\tau_j)$ . Suppose that exactly one segment  $\gamma_k$  is a null geodesic and that it lies in a geodesically convex neighborhood. Let the curve  $\Gamma_\epsilon(\tau)$  be the unique geodesic defined on the interval  $[\tau_k, \tau_{k+1}]$  starting at  $P_k$  and terminating at  $P_\epsilon := \gamma_{k+1}(\tau_{k+1} + \epsilon)$  (see Fig. 4). For sufficiently small  $\epsilon$ ,  $\Gamma_\epsilon$  is non-null, for otherwise  $\gamma_{k+1}(\tau_{k+1} + \epsilon)$  would lie on the light cone of  $P_{k+1}$ , which is impossible if  $\gamma_{k+1}$  is non-null. As  $\epsilon \rightarrow 0$ ,  $\Gamma_\epsilon(\tau) \rightarrow \gamma_k(\tau)$  for  $\tau \in [\tau_k, \tau_{k+1}]$  (by the smoothness of the exponential map).

Let  $\alpha_k^{(\epsilon)}$  and  $\alpha_{k+1}^{(\epsilon)}$  denote the angles at the intersections  $\gamma_{k-1}$  with  $\Gamma_\epsilon$  and  $\Gamma_\epsilon$  with  $\gamma_{k+1}$ , respectively. Let  $S$  and  $T$  be the tangents to  $\gamma_{k-1}$  and  $\Gamma_\epsilon$  at  $P_k$ , let  $\tilde{S}$ ,  $\tilde{T}$  be the parallel transport of  $S, T$  along  $\Gamma_\epsilon$  to  $P_\epsilon$ , and let  $U$  be

tangent to  $\gamma_{k+1}$  at  $P_\epsilon$ . Note that  $\tilde{T}$  is the tangent to  $\Gamma_\epsilon$  at  $\Gamma_\epsilon(\tau_{k+1})$  since  $\Gamma_\epsilon$  is geodesic. Parallel transport preserves angles (since it preserves inner products), and thus  $\alpha_k^{(\epsilon)}$  is equal to the angle from  $\tilde{S}$  to  $\tilde{T}$ . By additivity of angles,  $\alpha_k^{(\epsilon)} + \alpha_{k+1}^{(\epsilon)}$  equals the angle from  $\tilde{S}$  to  $U$ . By continuity of parallel transport with respect to initial conditions, as  $\epsilon \rightarrow 0$ ,  $\alpha_k^{(\epsilon)} + \alpha_{k+1}^{(\epsilon)}$  converges to the angle across the null geodesic  $\gamma_k$ .

Apply the Gauss-Bonnet formula of [30] to the modified curve  $\gamma_\epsilon$  which follows  $\gamma$  until time  $\tau_k$ , then follows  $\Gamma_\epsilon$  till  $\tau_{k+1}$ , then resumes following  $\gamma$  for all remaining time. By the remarks of the above paragraph, the sum of angles of  $\gamma_\epsilon$  converges to that of  $\gamma$ . Since  $\gamma_k$  and  $\Gamma_\epsilon$  are both geodesic, the geodesic curvature of  $\gamma_\epsilon$  differs from that of  $\gamma$  only on a short segment of  $\gamma_{k+1}$ , so that  $\oint_{\gamma_\epsilon} k_g ds$  converges to  $\oint_\gamma k_g ds$  also. Lastly, the sectional integral for  $\gamma_\epsilon$  differs from that of  $\gamma$  only by a wedge shaped region with vanishing area as  $\epsilon \rightarrow 0$ . Thus each term in the Gauss-Bonnet formula for  $\gamma_\epsilon$  separately converges to that with our definition of angle across a null geodesic, proving our generalized Gauss-Bonnet theorem in this case.

If the boundary curve  $\gamma$  has multiple null geodesics, inductively applying the same construction proves that the Gauss-Bonnet formula holds in this case as well.

We make two remarks on subtleties of applying Gauss-Bonnet in special cases: First, any spacetime surface bounded by the AI may be used to compute the sectional curvature integral. If the surface is deformed in the ambient 3+1 dimensional spacetime, the sectional curvature witnessed at particular points will of course vary, but the integrated curvature must remain fixed. This allows some flexibility in choosing convenient surfaces for calculation. Second, in dimensions higher than 1+1, it may happen

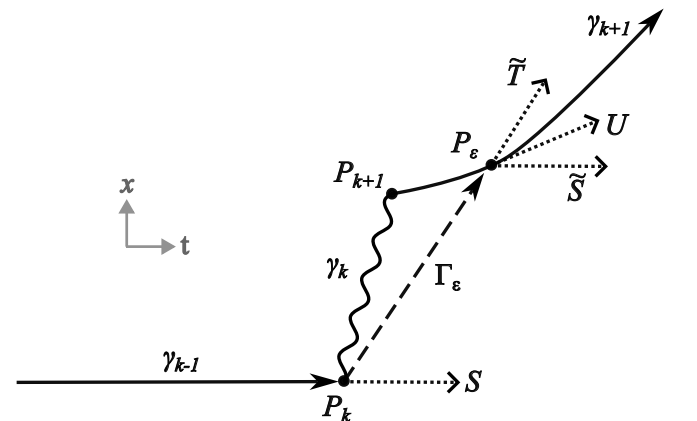


FIG. 4. Approximating a null geodesic segment  $\gamma_k$  by a non-null geodesic segment  $\Gamma_\epsilon$ . See text for definitions. Dotted lines indicate tangent vectors, solid lines are segments of the original path  $\gamma$ , and a dashed line is used for  $\Gamma_\epsilon$  only. For visual clarity, the tangent vector  $T$  has been omitted, as it would overlap with  $\Gamma_\epsilon$ .

that the same atom optics null geodesics do not address both arms of the AI. In this case, the Gauss-Bonnet formula may be applied to a loop formed by the AI arms,

two null geodesic segments associated with the trajectories of FBS photons which address the two AI arms, and a short spacelike segment connecting these two null segments.